https://doi.org/10.18524/1810-4215.2025.38.340350

DESIGN AND INVESTIGATION OF A NOVEL GAMMA-RAY SPECTROGRAPH CONFIGURATION IN THE ENERGY RANGE 0.511–5 MEV

Marko Doikov

Paisii Hilendarski University of Plovdiv, Faculty of Physics and Technology,
Tzar Asen St, 4000 Plovdiv, Bulgaria, *marik.doikov@gmail.com*

ABSTRACT. A novel composite gamma-ray detector based on three $CsPbBr_3$ crystals is proposed for the registration of quanta in the 0.1–5.0 MeV energy range. The central crystal simultaneously performs two functions: direct detection of gamma photons with energies up to 0.6 MeV and detection of annihilation-induced radiation in the 1.022–5.0 MeV range. The induced radiation is additionally recorded by two symmetrically positioned side crystals.

Monte Carlo simulations of gamma-ray transport within the primary crystal were performed to determine the detector response function and the angular scattering angular distribution. The secondary radiation yield and its detectability by the side detectors were quantified. Characteristic time constants of the detection processes and saturation regimes were identified. Furthermore, the economic feasibility of the proposed detector configuration was assessed, demonstrating its potential for practical implementation in advanced gamma-ray spectrographs.

Keywords: gamma-ray spectroscopy, $CsPbBr_3$ detector, positron annihilation, Monte Carlo simulation, composite detector design.

АНОТАЦІЯ. Запропоновано новий комбінований гамма-детектор на основі трьох кристалів $CsPbBr_3$ для реєстрації квантів у діапазоні енергій 0,511–5,0 МеВ. Центральний кристал виконує одночасно дві функції: безпосередню реєстрацію гамма-фотонів з енергіями до 0,6 МеВ та детекцію випромінювання, індукованого анігіляцією, у діапазоні 1,022–5,0 МеВ. Індуковане випромінювання додатково реєструється двома симетрично розташованими бічними кристалами.

Було виконано моделювання транспорту гамма-квантів у первинному кристалі методом Монте-Карло для визначення функції відгуку детектора та індикатриси кутового розсіяння. Оцінено вихід вторинного випромінювання та його реєстрація бічними кристалами. Визначено характерні часові константи процесів детектування та режими насичення. Додатково проведено аналіз економічної доцільності запропонованої конфігурації детектора, що демонструє її потенціал для практичного впровадження у сучасній гамма-спектрографії. Були визначені критичні режими роботи та розрахована реакція системи у вигляді імпульсів струму – дані, необхідні для проектування електронного інтерфейсу.

Ключові слова: гамма-спектроскопія, детектор $CsPbBr_3$, анігіляція позитронів, моделювання Монте-Карло, комбінована конструкція детектора.

1. Introduction

Detailed gamma-ray spectra became widely accessible to a broad range of specialists with the advent of semiconductor crystals possessing average atomic numbers Z in the range of 50–60 (Doikov, 2022). The high accuracy of the acquired spectral data, combined with the absence of a need for cryogenic cooling of gamma spectrographs, has significantly enhanced their availability and reduced production costs. Crystals and powders of $CsPbBr_3$ are now commercially available. γ- radiation with energies not exceeding 0.6 MeV can be efficiently detected using a crystal with a volume of ~1 cm^3. Under these conditions, γ-quanta in the intermediate energy range of 0.6–1.022 MeV require additional considerations for signal formation, as they are only partially absorbed within the crystal. Consequently, the efficiency of converting the absorbed photon energy into a current pulse is reduced.

The dominant interaction mechanism for γ-quanta, as illustrated in the figures presented in this study, is Compton scattering. For example, a single scattering event of an X-ray quantum with energy 50 keV results in a maximum energy transfer of approximately 5 keV. After undergoing multiple scattering events, low-energy X-ray and γ-quanta ($E_\gamma \leq 10$ keV) are subject to enhanced photo absorption (Liu et al, 2022; Weber) For effective absorption of γ-quanta in the range 0.6 MeV $\leq E_\gamma \leq$ 1.022 MeV, it is necessary to increase the thickness of the $CsPbBr_3$ absorber crystal. However, this approach contradicts the requirements for the miniaturization of gamma spectrographs. In this energy region, Compton scattering events become rarer, yet the resulting current pulse amplitude is significantly larger than that produced by absorbed photons in the lower-energy range 0.1 MeV $\leq E_\gamma \leq$ 0.6 MeV.

The present work is devoted to a novel method for recording gamma-ray spectra in the energy interval 1.022 MeV $\leq E_\gamma \leq$ 5 MeV. The implementation of this method is structured into three main stages, described in

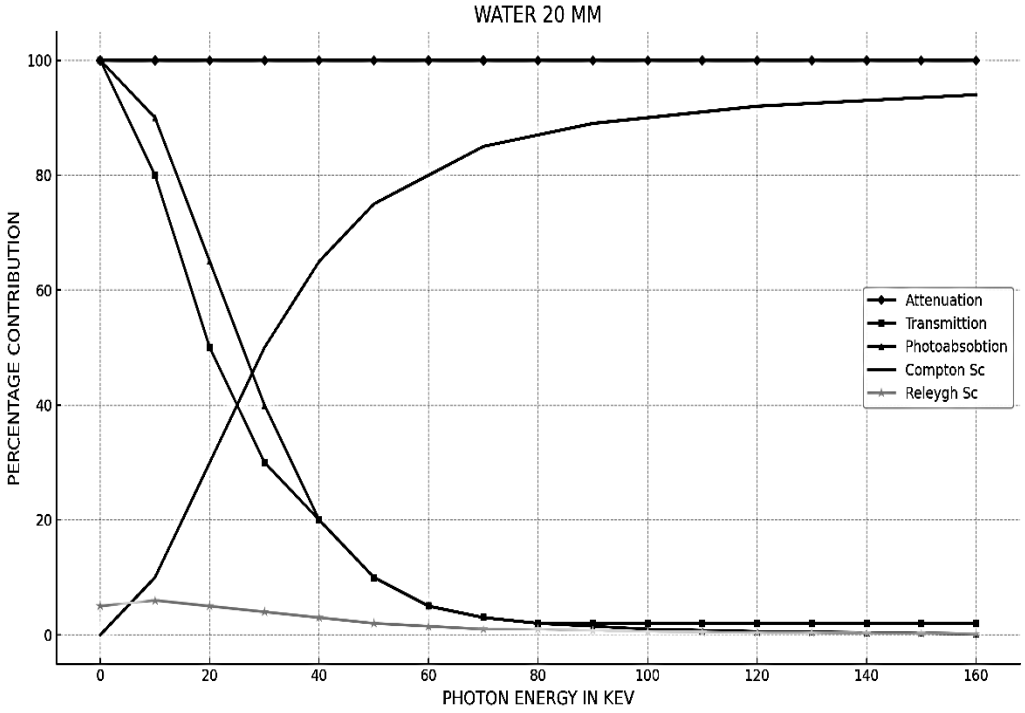

Figure 1: Interaction X-ray and γ-quanta with water

separate sections. Section 2 presents calculations of Compton scattering diagrams and the resulting angular distributions of γ-quanta, based on the Klein–Nishina formalism. Section 3 focuses on the calculation of cross-sections for electron–positron pair production in the vicinity of atomic nuclei in soft tissues. Importantly, the proposed method does not require increasing the thickness of the detector's absorbing layer. Section 4 discusses the detector design and its electronic interface. Sections 5 and 6 contain the Discussion and Conclusion, respectively, including a comparison of the developed device with previously reported detectors and the presentation of model gamma spectra.

2. Compton Scattering of γ-quanta in $CsPbBr_3$ Crystals

The propagation of X-ray and γ-quanta in matter is accompanied by photo absorption, collisions, and scattering processes, primarily Compton and Rayleigh scattering on atomic electrons (Weber; Incerti et al., 2010). Figure 1 illustrates the relative contributions of these interaction mechanisms during photon transport in soft tissues.

Photo absorption is most effective in the soft X-ray energy range. In the soft to intermediate gamma-ray range, inelastic Compton scattering dominates. From the Klein–Nishina equation, the angular scattering distribution (angular distribution) of γ-quanta can be derived.

$$\frac{d\sigma}{d\Omega} = \frac{r_0^2}{2}\left(\frac{E'}{E}\right)^2\left(\frac{E'}{E} + \frac{E}{E'} - sin\theta\right) \quad (1)$$

Here, θ denotes the scattering angle relative to the initial photon propagation direction. E' and E represent the energies of the scattered and incident photons, respectively, while r_0 is the classical electron radius. The angle θ also characterizes the electron scattering geometry.

The mean free path of X-ray quanta increases with photon energy. For photons with an energy of approximately 50 keV, the mean free path is about 8 cm. When compared to the dimensions of the phantom–represented here by a standard water phantom of 10^3 cm^3 volume – it can be concluded that, on average, a single scattering event occurs.

As shown in Table 1, approximately 30–40% of the scattered quanta possess a lateral, in particular perpendicular, component. For a soft-tissue thickness of 10 cm, the resulting fractional distribution is as follows: 70–80% of the photons remain unattenuated and do not interact, 10–20% undergo photo absorption, and among all scattered photons, 30–40% are deflected laterally. This corresponds to about 3–8% of the total photon flux. With increasing photon energy E, the scattering angular distribution E' becomes more strongly localized around the original photon propagation direction, as illustrated in Figure 2.

Table 1: Single scattering in soft tissues (water) at an X-ray energy of E = 50 keV. Percentage of scattered radiation:

Scattering angle θ (degrees)	Normalized dσ/dΩ
0° (forward)	1.0
45°	0.70
90° (lateral)	0.40
135° (backward)	0.15
180° (backward)	0.05

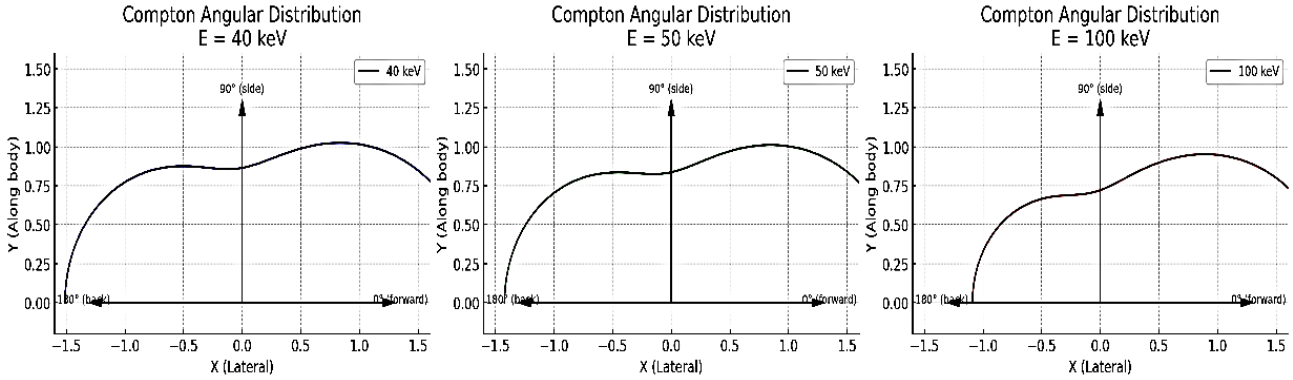

Figure 2: Scattering angular distribution of photons with different energies in the soft gamma-ray and hard X-ray range. The length of the line connecting the origin to a point on the diagram is proportional to the scattering probability.

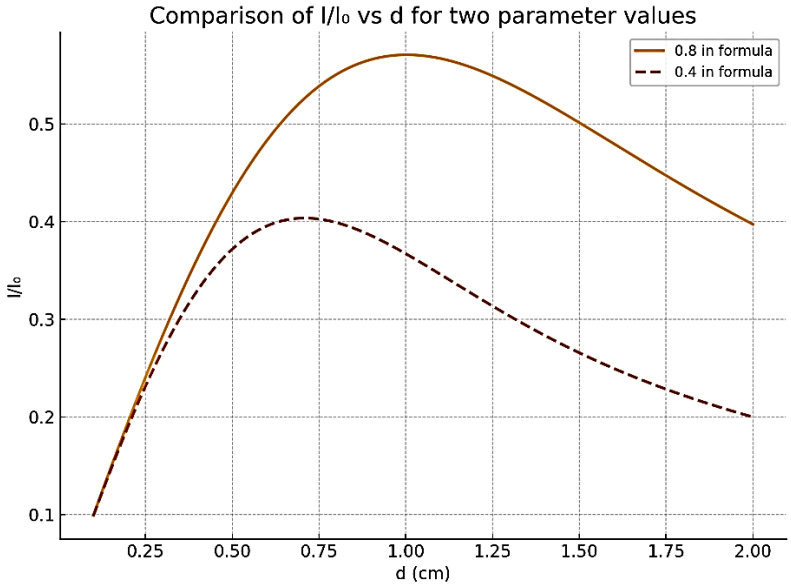

Figure 3: Dependence of $\frac{I}{I_0}$ on the crystal thickness d, calculated using the Hurst relation for characteristic potential differences V=500 V and V=1000 V $\mu\tau V = 0.4\ and\ 0.8$ in free dimension units).

The fraction of photons scattered in the forward direction increases with rising energy E. To calculate the current pulse, it is necessary to determine the energy $\Delta E_c = E - E' \approx (5-10)\ keV$. Let the band gap width of the $CsPbBr_3$ semiconductor be denoted as ΔE_{forb}. Then, the total number of electrons transferred from the valence band to the conduction band after a single inelastic scattering event is given by the expression:

$$N_{fr} = \Delta E_c / \Delta E_{forb}. \quad (2)$$

To calculate the amplitude of the current pulse, the relations provided in (Doikov, 2022, 2023), which are also relevant for the present study, were employed:

$$N_{fr} = \frac{\Delta E_c\left(1-exp\left(-k_\gamma d\right)\right)}{\Delta E_{forb}} \quad (3)$$

In the exponent, it is more convenient to replace the extinction coefficient of gamma or X-ray radiation k_γ with the mass extinction coefficient $k_\gamma(m)$. The value of $k_\gamma(m)$ allows one to evaluate the percentage contribution of various scattering and absorption mechanisms to the total extinction, for example, in soft tissues (see Fig. 1). For semiconductor crystals of $CsPbBr_3$, the effective average atomic number is $M_\mu = 57.35$. The mean mobility–lifetime product of electron–hole pairs is $\mu\tau = 8 \cdot 10^{-4} cm^2/V$ where V denotes the potential difference between the electrodes of the $CsPbBr_3$ crystal. The signal-to-noise ratio, in the first approximation, can be expressed by the Hurst relation, which is useful for physical analysis:

$$\frac{I}{I_0} = \frac{\mu\tau V}{d}\left(1 - exp\left(-\frac{d^2}{\mu\tau V}\right)\right) \quad (4)$$

or alternatively, by incorporating the semi-empirical data reported in (Zhang,Zhou, 2020; Liu, Wu, Wei, et al., 2022; López, Abia, Consuelo et al., 2020).

$$\frac{I}{I_0} \approx \frac{0.8}{d}\left(1 - exp\left(-\frac{d^2}{0.8}\right)\right) \quad (5)$$

Here, the quantity on the left-hand side of the equation, $\frac{I}{I_0}$, represents the relative reduction (or change) in the current when passing through a layer of thickness d. This ratio describes the attenuation of current (or radiation, or signal) due to the presence of a material layer into which charges, photons, or ions penetrate. In detector physics (for example, in scintillation layers), the ratio $\frac{I}{I_0}$ can be associated with the particle detection efficiency as a function of the active layer thickness.

Numerous measurements of the aforementioned parameters have demonstrated that the optimal thickness d of $CsPbBr_3$ crystals corresponds to the values at which the plotted function reaches its maximum. This fact determines the characteristic dimensions of commercially available detector-grade crystals. The signal-to-noise ratio in modern $CsPbBr_3$ based detectors typically ranges from 80 to 100, making them competitive with more expensive counterparts based on other crystals containing heavy elements. Asymptotic behavior: when $d \ll \lambda$, where $\lambda = \mu\tau V$, almost the entire intensity is transmitted. For $d \gg \mu\tau V$, $\frac{I}{I_0} \approx \frac{\mu\tau V}{d}$ i.e., the intensity decreases inversely with thickness.

3.1. Quantitative estimates of elementary processes within the specified energy range

3.1.2. Expected current response. We introduce the following notation:

- Q – the charge of the electron cloud generated by the passage of a single ionizing gamma or X-ray quantum. The value of Q includes secondary electrons and holes (the avalanche multiplication is ensured by the high potential difference V applied to the contacts, typically (500–1000 V).
- τ_{drift} – the charge drift time in the $CsPbBr_3$ crystal, with $\tau_{drift} \approx 10\ ns$, E_{dep} – the absorbed energy corresponding to the four primary interaction mechanisms,

$$E_{dep} \approx 1.022 MeV - 6\ MeV \approx (1.022 - 6) \cdot 10^6\ eV \quad (6)$$

- $\Delta E_{el+dot} \approx 10\ eV - 25\ eV$ – the average energy required to generate an electron–hole pair (including possible trapping states).

Under these assumptions, the current response induced on the electrodes can be estimated for the given ionization parameters as:

$$E_{dep} \approx 5 \cdot 10^6\ eV; Q = \frac{E_{dep}}{\Delta E_{el+dot}} =$$
$$= 4 \cdot 10^{-14}\ Ql;\ \ I(\tau_{drift}) = \frac{Q}{\tau_{drift}} \approx 4\ \mu A \quad (7)$$

The obtained results are essential for evaluating the amplitude of the current pulse. Within a single significant order of magnitude, the values of the maximum amplitudes $I(\tau_{drift})$ vary. An analysis of the current amplitudes shows that $I(\tau_{drift})$ deviates significantly from a symmetric signal shape (Doikov, 2023). This demonstrates the practicality of integrating the pulse and subsequently discretizing it by the total charge Q. In this case, the current pulse is transformed into a standard rectangular shape and further converted into a potential pulse. The output values of the processed gamma spectrum exhibit high physical reliability.

With complete absorption of a γ-quantum with an energy of 5 MeV via pair production, a $CsPbBr_3$ detector can generate a peak current on the order of 4–8 μA, with a duration of approximately 10–20 ns, depending on the carrier mobility and the applied electric field. Let us examine in more detail the absorption capability of $CsPbBr_3$ crystals and soft tissues in connection with the need to address a range of applied problems. Water-containing aerosols in thunderclouds actively interact with gamma radiation. The deceleration of electrons in the fields of oxygen, nitrogen, and hydrogen atoms leads to the emission of continuous gamma quanta of sufficiently high energies. The electric potential of a lightning discharge can reach about 200 MeV. Therefore, the flux of gamma quanta is sufficient to produce electron–positron pairs in the electric field of a thunderstorm discharge (in water vapor). At lightning branch points, synchrotron X-ray and, more rarely, gamma radiation have also been observed. Thus, lightning provides conditions for bursts of direct gamma radiation. After interacting with nuclear fields, such gamma quanta with $E_\gamma \geq 1.022\ MeV$ E vanish, resulting in the creation of electron–positron pairs.

Fig. 4 also shows the current response of a $CsPbBr_3$ crystal in the energy range 1.022–5 MeV. The following contributions are taken into account: Direct ionization (a gradual increase with energy); Pair production (a sharp quadratic rise above 1.022 MeV); Total signal, which becomes increasingly dominated by the pair-production contribution at energies above approximately 2.5 MeV. The comparative contribution of electron–positron pair production to the formation of the current pulse is presented in Fig. 5. The ionization losses from the creation of electron–positron pairs are formed by the beta electron of the pair, the positron, and two annihilation γ-quanta with energies of 0.511 MeV, which in turn contribute to the current pulse. From the law of energy conservation, the residual kinetic energy of the produced particle pair must also be taken into account.

The dashed curve represents the current from the two 511 keV γ-quanta produced during positron annihilation (this contribution remains constant above the 1.022 MeV threshold). The black dash-dot curve shows the total detector response, taking into account: direct ionization, pair production, annihilation radiation. This contribution is particularly noticeable in the 1.5–2.5 MeV region, before the main energy losses from the electron–positron pairs themselves become dominant.

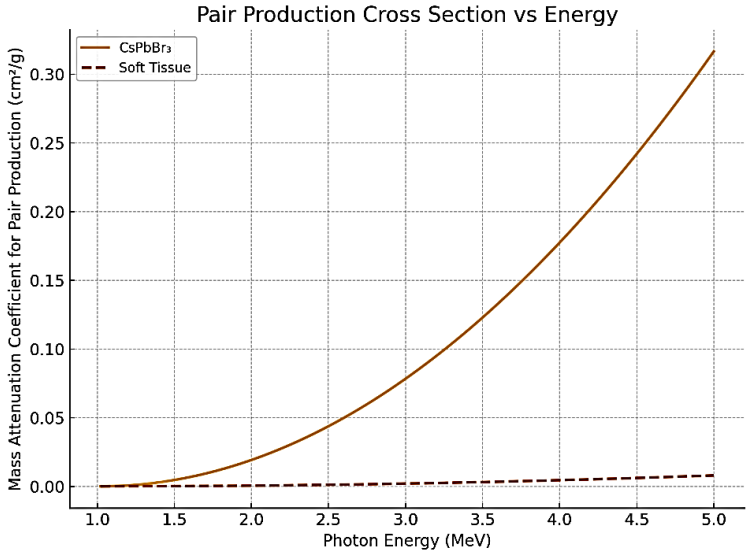

Figure 4: Extinction of gamma quanta with $1.022\ MeV \leq E_\gamma \leq 5\ MeV$ in soft tissues (Water) and in $CsPbBr_3$ crystals.

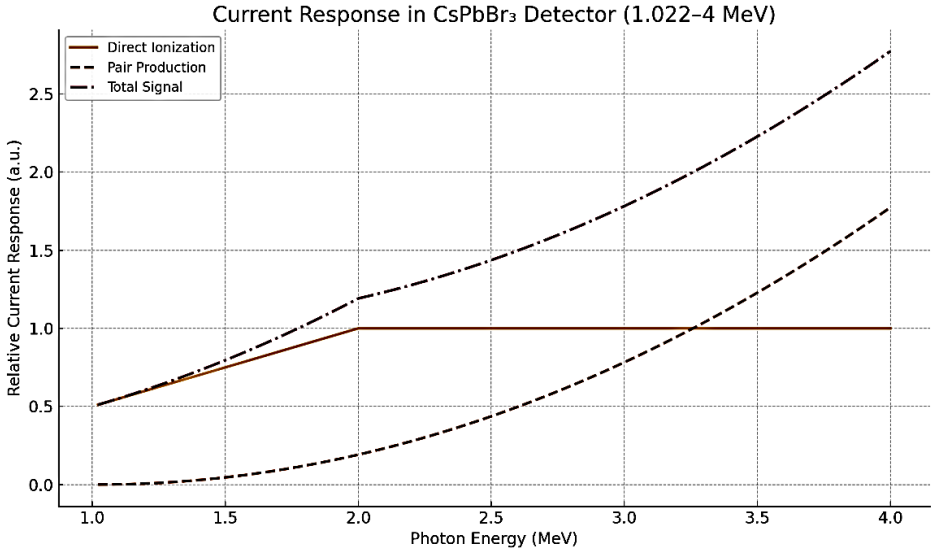

Figure 5: Relative contribution of annihilation to the resulting current response.

3.1.3. Accounting for incomplete absorption of annihilation-induced quanta. Consider a $CsPbBr_3$_33 crystal irradiated by γ-quanta with energies from 1.022 MeV to 4 MeV. The crystal volume is 1 cm³. We aim to determine the relative fraction of emitted γ-quanta generated as a result of electron–positron pair production near the nuclei constituting the crystal. To evaluate the relative yield of annihilation γ-quanta (511 keV) produced during the creation of electron–positron pairs in a $CsPbBr_3$ crystal of volume 1 cm³, we define the percentage of γ-quanta escaping the crystal – i.e., those not absorbed after positron annihilation – as a function of the energy of the primary γ-quantum that initiated the pair production process.

Material: $CsPbBr_3$, density ≈4.9 g/cm³, geometrical shape – cube of 1 cm³. The mass extinction coefficient is $\frac{\mu_{ext}}{\rho} = 0.25\ cm^2/g$. Thus, the linear extinction coefficient is $\mu_{ext} \approx 0{,}25 \cdot 4{,}9 \approx 1{,}225\ cm^{-1}$. The mean free path is therefore λ=1/μ≈0.816 см. The final step is to calculate the survival (escape) probability – P_{esc} of a γ-quantum with energy $E_\gamma = 0{,}511$ MeV:

$$P_{esc} = \frac{1}{6}\int_0^1 exp\left(-\frac{x}{\lambda}\right)dx = \lambda\left(1 - exp\left(-\frac{1}{\lambda}\right)\right) \approx 0{,}293 \quad (8)$$

Conclusions for this section. Approximately 29.3% of the annihilation γ-quanta generated within a 1 cm³ volume of $CsPbBr_3$ escape the crystal without being absorbed.

Approximately 80% of the total number of annihilated quanta, as well as the resulting combined contribution to the detector pulse. In the final figure, it is taken into account that about 29.3% of the annihilation γ-quanta generated within a 1 cm³ volume of $CsPbBr_3$ escape the crystal without being absorbed. Having obtained the final results (Fig. 7), we now proceed to the development and modeling of a combined gamma detector.

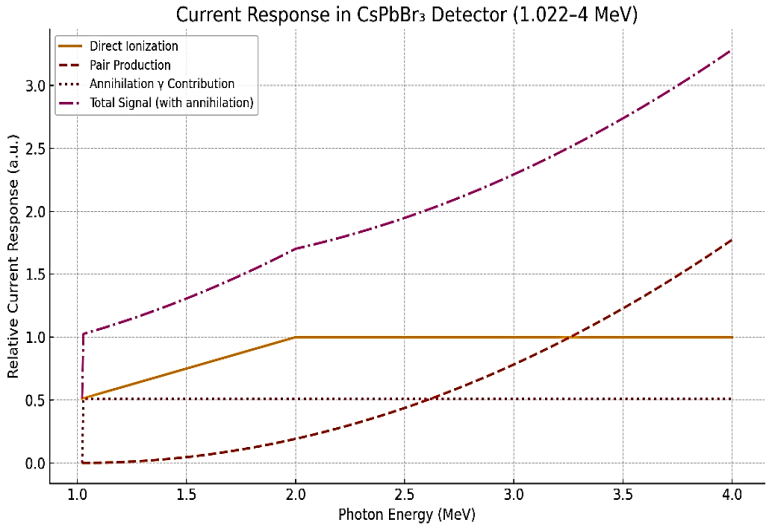

Figure 6: Current response of the detector accounting for direct ionization, electron–positron pair production, annihilation, and the resulting combined contribution to the detector pulse.

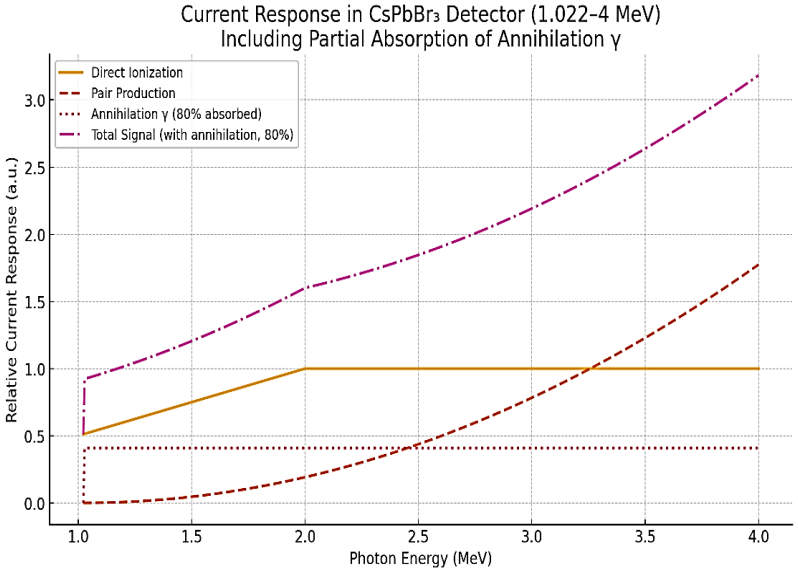

Figure 7: Current response of the detector accounting for direct ionization, electron–positron pair production, and annihilation.

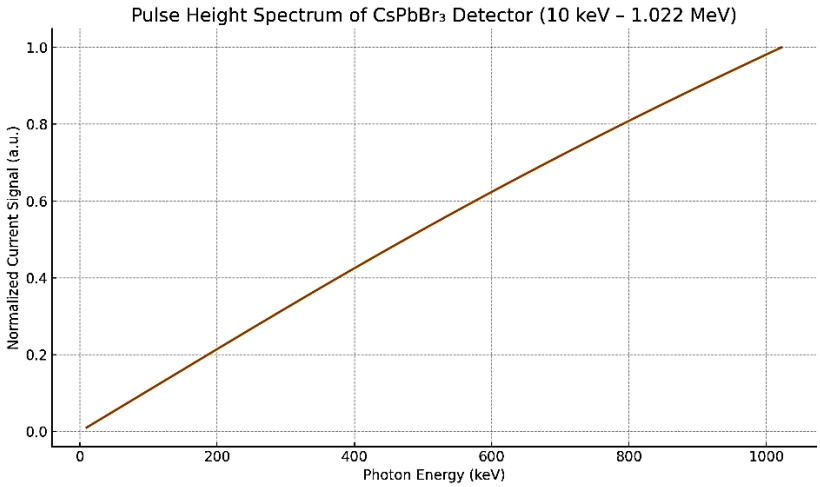

Figure 8: I(t)[a.u.] = Q(t)/Qmax – normalized current signal.

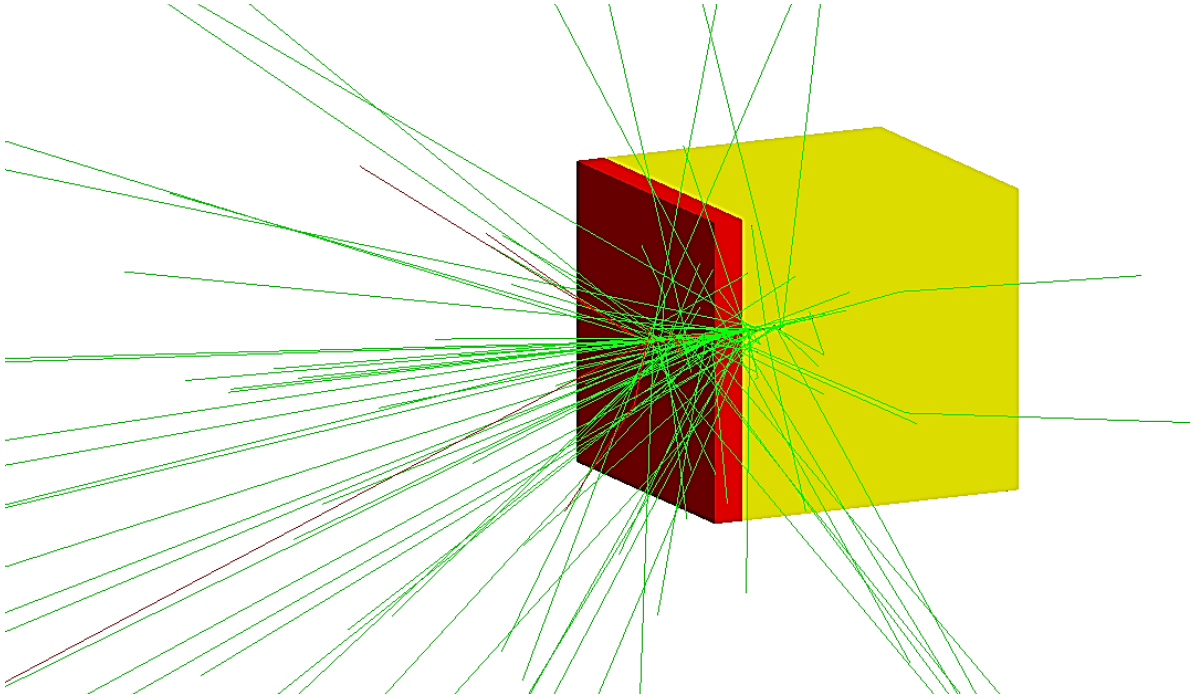

Figure 10: Simulation of a $CsPbBr_3$ crystal detector with a beam of 1000 γ-quanta.

4. Design of a combined detector

In this section, the most technically challenging task is the development of a gamma detector capable of reconstructing the spectra of investigated objects in the energy interval 0.511–1.022 MeV. Within this range, only ionization losses caused by Compton scattering need to be considered. Figure 4 presents the results of quantitative calculations of the total absorption coefficient. It should be noted that most radioactive isotopes exhibit their activity in the form of both discrete (line) spectra and Compton continua, analogous to the presence of discrete spectral lines superimposed on a continuous background in classical optics. The graph shows the spectrum of current pulses from a $CsPbBr_3$ – based detector with a volume of 1 cm^3 when interacting with γ-quanta with energies from 10 keV to 1.022 MeV.

The key features of the normalized current pulse dependence are determined by the efficiency of gamma-quantum extinction mechanisms, more precisely by the slope of the curve in Fig. 4. In particular: At low energies (up to ~100 keV), the current is small due to the high probability of transmission without interaction. In the range 200–600 keV, the response increases sharply due to more efficient absorption, primarily through the photoelectric effect. As the energy approaches 1 MeV, the current continues to grow but with a reduced slope, as the interaction probability begins to decrease. This spectrum represents not an energy-dispersive response, but rather the current (pulse) response. When gamma spectra need to be studied, a practical solution would involve considering both the intrinsic energy resolution of the detector and the spectrum of the incident radiation.

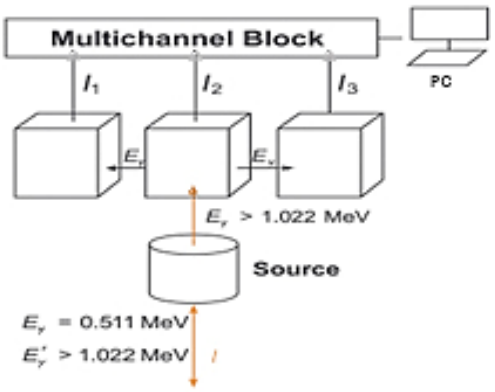

Figure 9: Schematic view of the gamma spectrograph for induced radiation.

5. Discussion

The diagnostics of physical media using next-generation high-precision gamma and X-ray spectrographs significantly expands the range of solvable problems in medicine, meteorology, and astrophysics. γ-quanta are formed by two independent mechanisms. For example, in Fig. 6, 7 a directed flux of beta particles and Gamma rays is emitted from a shielded cylindrical container. The device incorporates three independent detectors: the central detector records the direct radiation, while the lateral crystal semiconductor detectors register induced γ-quanta of strictly defined energy - 0.511 MeV.

For the "purity" of the experiment, it is necessary to determine the fraction of the scattered component of the flux that reaches the lateral detectors. For this purpose, the

results of standard modeling of multiple scattering of quanta within a CsPbBr3 crystal are used. It should be noted that the fraction of scattered quanta increases with decreasing energy of the incident quanta. When the photon energy Eγ increases such that $E_\gamma \gg 0.1$ MeV, the angular distribution becomes dominated by forward Compton scattering, as is evident in Fig. 2 for $E_\gamma =$ 0.1 MeV. Therefore, the effect of induced emission of gamma quanta can be considered "free" of scattered quanta from the direct flux.

In comparison with traditional CdZnTe and $LaBr_3$(Ce) detectors, the proposed $CsPbBr_3$ configuration provides the same or even better energy resolution (~1–2% FWHM at 662 keV) and higher detection efficiency in the 0.511–5 MeV range due to active capture of annihilation photons and operation at room temperature without cryogenic cooling. $CsPbBr_3$ crystals are inexpensive and readily available, and their composite geometry (central and side crystals) allows for efficient detection of 511 keV photons, eliminating escape peaks and expanding the measurable energy range. Thus, this design combines the resolution of semiconductors, the efficiency of scintillators, and low cost, representing a new generation of compact gamma spectrographs. The maximum permissible flux of gamma quanta is limited to approximately $10^6\,см^{-2}s^{-1}$. At this level, the detection system is unable to fully relax to its initial state between successive events. To calculate the response curve of $CsPbBr_3$ and predict the pulse shape generated by individual gamma or X-ray quanta, we employed the open-source Geant4-DNA v11.2 simulation toolkit (Incerti et al., 2010), as utilized during participation in the International Geant4 School, Pavia, Italy (January 11–19, 2024).The trajectory of each quantum within the $CsPbBr_3$ crystal is governed by its chemical structure and by fundamental processes such as absorption, scattering, and pair production. The Monte Carlo method implemented in Geant4 regulates the elementary interactions of photoabsorption, Compton and Rayleigh scattering, and electron–positron pair creation. The absorbed dose – resulting from both the primary quanta and the secondary photons and particles they generate – forms a current pulse in both the primary and secondary detectors. According to the performed calculations, the amplitude and shape of the current pulse within the principal operational range of radiation fluxes exhibit a linear dependence on the absorbed dose. The proposed combined detector allows separate construction of spectra for primary and secondary radiation components. Solving this problem by alternative analytical methods is practically impossible.

6. Conclusion

The gamma spectrograph for induced radiation has made it possible to broaden the range of applied tasks. This work proposed new configurations, structural elements, and physical principles that allow the exploitation of detectors composed of atoms with high atomic weights. The absence of a need for deep cooling and the commercial availability of $CsPbBr_3$ crystals make their mass production feasible and enable their wide implementation in nuclear medicine and geophysics. A complete set of simulations of the expected parameters of the developed detectors was carried out with the goal of fabricating a prototype. Critical operating modes were determined, and the system response in the form of current pulses was calculated—data necessary for the design of the electronic interface.

Acknowledgment. The author expresses sincere gratitude to Senior Researcher of INFN Luciano Pandola for his support of the present work, to Prof. V. Ya. Gotsulski for his critical remarks, to Prof. Slavi Ljubomirov (Plovdiv University, Bulgaria), and to Prof. Dmitri Doikov (Department of Physics, Medical Laboratory, Medical Center Tzafon, Poria, Israel) for their guidance and supervision of the study.

References

Doikov M.: 2022, *OAP*, **35**, 24. DOI: 10.18524/1810-4215.2022.35.268000

Doikov M.: 2023, *OAP*, **36**, 42. DOI: 10.18524/1810-4215.2023.36.290774

Incerti S. et al.: 2010, *IntJModSimulSciCom*, **01**, 02, 157. https://doi.org/10.1142/S179396231000012

Liu Fangze et al.: 2022, *ACSEnL*, **7**, 1066. https://doi.org/10.1021/acsenergylett.2c00031

López Carlos A. et al.: 2020, *ACSOmega*, **5**, **11**, 5931. DOI: 10.1021/acsomega.9b04248.

Weber G. https://web-docs.gsi.de/~stoe_exp/web_programs/x_ray_absorption/index.php

Zhang Huan, Zhou YouHe: 2020, *NatCo*, 11, id. 5072 https://www.nature.com/articles/s 41467020187590